Determination of Z_{eff} by integrating measurements from x-ray tomography and charge exchange recombination spectroscopy

Determination of Z_{eff} by integrating measurements from x-ray tomography and charge exchange recombination spectroscopy

M.E. Galante[1], L.M. Reusch[1], D.J. Den Hartog[1], P. Franz[2], J.R. Johnson[1], M.B. McGarry[1], M.D. Nornberg[1] and H.D. Stephens[1,3]

[1] University of Wisconsin-Madison, Madison, WI 53706, USA
[2] Consorzio RFX, Associazione EURATOM-ENEA sulla Fusione, Padova, Italy
[3] Pierce College Fort Steilacoom, Lakewood, WA 98498, USA

E-mail: galante@wisc.edu

CrossMark

Abstract

The effective ionic charge, Z_{eff}, is determined through the integration of soft x-ray tomography and charge exchange recombination spectroscopy impurity density measurements in the Madison Symmetric Torus. Z_{eff} is found is be 2.3 ± 0.1 in the core of high temperature, high current, improved confinement discharges, with a slightly hollow profile peaking near mid-radius. A Bayesian probability framework, developed as part of an on-going effort in Integrated Data Analysis, was used to incorporate these two measurements. This framework provides a method to address different systematic and statistical uncertainties associated with each diagnostic and to test hypothetical contributions to Z_{eff} against the existing data set. The combined analysis provides much higher confidence in the result than previous single-diagnostic attempts to characterize Z_{eff} using near-infrared bremsstrahlung or x-ray spectroscopy.

Keywords: Z_{eff}, SXR tomography, CHERS, integrated data analysis, Bayesian probability theory

(Some figures may appear in colour only in the online journal)

1. Introduction

The effective ionic charge (Z_{eff}) is a critical, though difficult to measure, parameter in high temperature plasma physics. Along with the electron temperature (T_e), it determines the plasma resistivity, which plays a key role in Ohmic power absorption and energy confinement time. Due to its importance, significant efforts have been made both experimentally and computationally to determine Z_{eff} in the Madison Symmetric Torus (MST). However, no single diagnostic currently available on MST is able to provide an accurate measurement of Z_{eff}. Standard visible and near-infrared bremsstrahlung techniques were found to be contaminated with both molecular and electron-neutral bremsstrahlung emission [1]. Previous

x-ray studies, coupling x-ray spectroscopy measurements with Fokker-Planck modeling, did not incorporate the presence of recombination emission [2, 3]. Using soft x-ray (SXR) signals to determine Z_{eff} is a complicated task in most plasma experiments due to the signal's additional dependence on T_e and the electron and ion densities (n_e, n_i). More information is therefore needed to constrain sources contributing to the measured signal, e.g. bremsstrahlung, impurity recombination, and line emission. Charge exchange recombination spectroscopy (CHERS) provides an estimate of Z_{eff} by directly measuring the contribution of a given impurity. However, these measurements alone provide only a lower bound on Z_{eff} as it is impractical, if not impossible, to directly measure every impurity in a discharge.

While no one diagnostic can determine Z_{eff} on MST, it is possible to combine information from multiple diagnostics to produce an estimate. Integrated data analysis (IDA) is the concept that measurements from multiple, distinct diagnostics, along with their uncertainties, can be combined to produce the most probable value for a parameter of interest that is more precise than any of the diagnostics individually. This method takes advantage of diagnostic redundancy, that is, multiple diagnostics that all have some dependence on the same parameter, which enables determination of parameters that cannot be accurately measured by any single diagnostic. Best practices in science have long encouraged the use of multiple diagnostics to measure physical quantities, thus IDA is not a new concept. However, the lack of a rigorous framework with which to do this often stymies these practices. IDA within a Bayesian probability theory framework provides a systematic methodology for combining measurements. Such a framework has already been implemented on a number of fusion experiments to measure a variety of plasma parameters, including Z_{eff} [4–7].

Here, we present an estimate of Z_{eff} in high temperature improved confinement discharges in MST, determined by coupling SXR tomography and CHERS measurements. SXR measures all sources of x-ray emissivity produced by the plasma, including bremsstrahlung, radiative recombination and line emission. CHERS provides measurements of those impurity species that are present to contribute to the SXR signal and, when absolutely calibrated, the density of some of those species. By combining the information provided by each of the diagnostics a more complete measure of Z_{eff} is found. We believe this to be the first application of Bayesian probability theory and IDA to SXR measurements for Z_{eff}.

This paper is organized as follows. In section 2 we describe the experimental setup and major hardware used in these experiments. Bayesian probability theory is introduced in section 3. The synthetic SXR tomography diagnostic used for modeling is discussed in section 4. We present results for Z_{eff} in high current, high temperature, improved confinement discharges in section 5, along with a discussion of the results. Finally, in section 6 we present our conclusions and future work.

2. Apparatus

2.1. MST

The experiments presented in this work were conducted in the Madison symmetric torus (MST), a medium size reversed field pinch (RFP) with major radius $R = 1.5$ m, and minor radius $a = 0.52$ m [8]. The major impurities contributing to Z_{eff} in MST are carbon, aluminum, boron, oxygen, and nitrogen. The first three are sourced from plasma facing components. MST has an aluminum vacuum vessel with a carbon limiter that is in direct contact with the plasma. Boronization, as well as boron nitride probe covers introduce a non-negligible amount of boron to the plasma. Oxygen and nitrogen are atmospheric contaminants.

All results presented here were obtained in high current, high temperature, improved confinement discharges. The increase in confinement is achieved by application of a parallel edge current, which flattens the current profile and suppresses magnetic activity. This technique, known as pulsed parallel current drive (PPCD) [9, 10], produces core electron temperatures greater than 1 keV resulting in most low-Z impurities being fully ionized. The discharges chosen for analysis did not display significant 3D structures that are present in some MST plasmas.

2.2. SXR tomography

The SXR tomography system at MST is a mature diagnostic that is routinely used as part of MST's extensive diagnostic suite. The system measures broadband x-ray emission composed mainly of bremsstrahlung and radiative recombination in the 2–8 keV energy range along 40 unique crossing lines of sight. Each line of sight is viewed through a pair of diodes that each look through a different thickness Be filter providing coarse energy resolution. The filters for all data presented in this work were 421 and 857 μm. These filter thicknesses were specifically chosen to block high energy line emission, primarily from He and H-like Al, thus the signal is composed primarily of bremsstrahlung and recombination radiation. The system has a temporal resolution of approximately 0.01 ms and a spatial resolution of approximately 2 cm. Additional details regarding the system can be found elsewhere [11]. Due to diagnostic considerations, specifically signal-to-noise ratio, the system is currently used primarily in high current PPCD plasmas.

2.3. CHERS

The CHERS system on MST consists of a 50 kV diagnostic neutral beam viewed perpendicularly by 11 chords at a single toroidal location. One chord per discharge is imaged onto a custom built duo spectrometer providing a single radial point, single species measurement. Multiple similar discharges are then ensembled to produce a radial profile. The system is used primarily for C^{+6} measurements, though measurements of B^{+5}, O^{+8}, Al^{+11}, and Al^{+13} have also been made. The spectrometer is absolutely calibrated for radiant sensitivity to provide a measure of impurity density from charge exchange brightness. The system has a temporal resolution of approximately 0.01 ms and a spatial resolution of approximately 2 cm. Further details of the system can be found elsewhere [12–14]. In PPCD, CHERS measurements indicate aluminum to be in its four highest charge states, Al^{+10}–Al^{+13} [15].

3. Bayesian probability theory

Bayesian probability theory (BPT) provides a mathematical framework for combining relevant information, including both statistical and systematic uncertainties, from each diagnostic to produce a probability distribution for the value of the parameter of interest. A complete treatment of BPT is beyond the scope of this work, however an excellent review can be found in Ref. [16]. Bayes' law, the basis for BPT, is
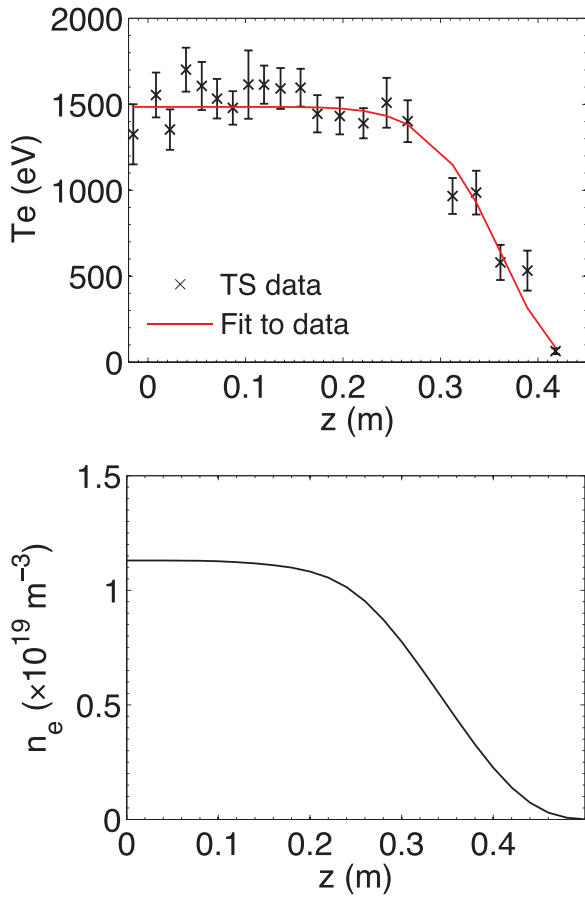
Figure 1. Example T_e (top) and n_e profiles from Thomson scattering and FIR interferometry, respectively, used in this work.

$$p(\theta|x,I) = \frac{p(x|\theta,I)p(\theta|I)}{p(x|I)} \qquad (1)$$

where p($\theta|x,I$), the posterior distribution function, is the probability of getting a parameter θ, given the data x, and any additional information I. $p(x|\theta,I)$ is the likelihood distribution, which describes the probability of getting x given θ. $p(\theta|I)$ is the prior distribution. For the work presented here the prior represents the range in which we expect the result to fall. $p(x|I)$ is a normalization factor known as the evidence. This technique is highly modular, enabling easy inclusion of many diagnostics through multiplication,

$$p(Z_{\text{eff}}|x,I) \propto p(x|Z_{\text{eff}},I)_{\text{SXR}} \times p(x|Z_{\text{eff}},I)_{\text{CHERS}} \times \text{etc}, \quad (2)$$

where each factor on the RHS is the likelihood distribution for a different diagnostic and we have assumed independence between the diagnostics, i.e. CHERS and SXR data are not correlated.

The likelihood function is a comparison between measured and predicted data through the use of a 'cost function'. For the SXR tomography system we assume a Gaussian likelihood

$$P(x|n_z,T_e,n_e,\sigma) = \frac{1}{\sqrt{2\pi}\,\sigma} \exp\left(-\frac{1}{2}\chi^2\right), \qquad (3)$$

with

$$\chi^2 = \frac{[b_{\text{data}} - b_{\text{mod}}(n_z,T_e,n_e)]^2}{\sigma^2}, \qquad (4)$$

where b_{data} is the measured brightness with uncertainty σ, and b_{mod} is the predicted brightness given n_z, T_e, and n_e. Maximizing the likelihood function, within the bounds of the prior distributions, returns the parameters that best match the model to the data. In this work, T_e and n_e are constrained by Thomson scattering and far infrared interferometry, respectively. Example T_e and n_e profiles are shown in figure 1. The impurity density (n_z) is allowed to vary until the model best matches the data.

A Markov Chain Monte Carlo (MCMC) search method was used to determine the parameters that returned the best fit between the model and the data. The method is very fast compared to a standard 'grid search' when using a large number of parameters, and returns the distribution for the parameters. Typically 8–10 parameters are used depending on the number of species modeled and whether the emissivity contains localized structures. Having a distribution function for each parameter enables consistent error analysis as the uncertainty in the best fit parameters can be found directly from the distributions. A similar method is currently being used at MST to determine T_e in an IDA framework using Thomson scattering and SXR measurements [17].

4. Synthetic diagnostic

In order to utilize BPT, a proper forward model is needed to calculate the expected measurements. An excellent relative SXR forward model exists at MST and is used to determine T_e from SXR using the double-foil technique [18]. However, the model does not predict the absolute SXR brightness as it assumes pure bremsstrahlung emission from the plasma. It is known that SXR signals in most high temperature plasma devices are contaminated by impurity emission [19]. Figure 2 illustrates that for MST relevant temperature, density and assumed impurities, the radiative recombination emissivity (dashed) is 2–3 times larger than the bremsstrahlung (solid) in the energy range of the SXR detectors.

To properly model the absolute SXR brightness, the existing forward model was modified to calculate the impurity recombination contribution. The space dependent x-ray emissivity due to recombination for a given impurity was modeled as [20]

$$\varepsilon = AG\frac{n_e n_i Z^2}{\sqrt{T_e}} \exp\left(-\frac{E}{T_e}\right)$$
$$\times \left[\frac{\xi}{n^3}\frac{\chi_i}{T_e}\exp\left(\frac{\chi_i}{T_e}\right) + \sum_{v=n+1}\frac{Z^2 R_y}{T_e}\frac{2}{v^3}\exp\left(\frac{Z^2 R_y}{n^2 T_e}\right)\right] \qquad (5)$$

where A is a physical constant (1.7×10^{-38}), n_e and n_i are the electron and impurity ion densities, respectively, T_e is the electron temperature, R_y is the Rydberg constant, Z is the ionic charge, G is the Gaunt factor (assumed 1 for x-rays), n is the principle quantum number of the lowest unfilled shell, ξ is the number of holes in the lowest unfilled shell and χ is the recombination energy. In the calculations presented here, the sum was
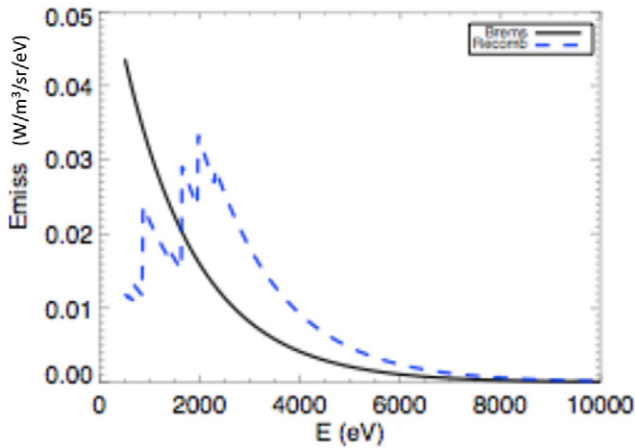
Figure 2. Estimated bremsstrahlung (black solid) and recombination (blue dashed) spectra for MST relevant temperature (1.5 keV), density (1×10^{19} m^{-3}) and impurity content. Recombination is the dominate emission source in the energy range of our detectors, 2–8 keV.

taken over the first five quantum states. The total recombination spectrum is the sum of the spectra from each impurity species

$$\varepsilon_{Rec,tot} = \varepsilon_{Rec,Z_I} + \varepsilon_{Rec,Z_{II}} + \varepsilon_{Rec,Z_{III}} + ... \quad (6)$$

This spectrum was then added to the bremsstrahlung spectrum that was calculated using Z_{eff} determined self-consistently for the included impurity species. The combined spectrum was then convolved with the transmission function of the Be filters and the response function of the detector, integrated over energy and integrated over the path length of the detectors to return a predicted SXR brightness for given T_e, n_e, n_z, and Z_{eff}.

The model takes the C^{+6} and Al^{+11} density profiles as inputs then calculates the best fit between the measured and modeled brightness for a given plasma temperature and density. All eight intrinsic impurity species are used in calculating the brightness, with empirically derived ratios for the densities $n_O/n_C = 0.9$, $n_B/n_C = 0.3$, $n_N/n_C = 0.3$ and the aluminum charge states given by ionization balance under the assumption of coronal equilibrium, as predicted by ADAS [21]. The ratios of impurity species, as well as the distribution of aluminum charge states, have been confirmed by CHERS measurements in similar discharges [15, 22]. Unknown impurities, i.e. those not directly measured by CHERS, can be included in the model to make up the difference between the model and data when the CHERS measurements are insufficient to describe the measured signals. This introduces an element of uncertainty into the determination of Z_{eff}, however it can provide an upper bound on the measurement of Z_{eff}. Additionally, this feature can be used for hypothesis testing, investigating the possibility that specific impurities are present in the plasma, contributing to the SXR signal.

All profiles are assumed to have the same shape, parameterized as

$$n(r) = n_0(1 - (r/a)^\alpha)^\beta + \Delta n \exp(-(\delta_r - r/a)^2/2\Delta r^2), \quad (7)$$

where n_0 is the core density, Δn is the amplitude of the density perturbation, δ_r is the location of the perturbation and Δr is the width of the perturbation. This model assumes a ring density structure, however an island structure can also be included
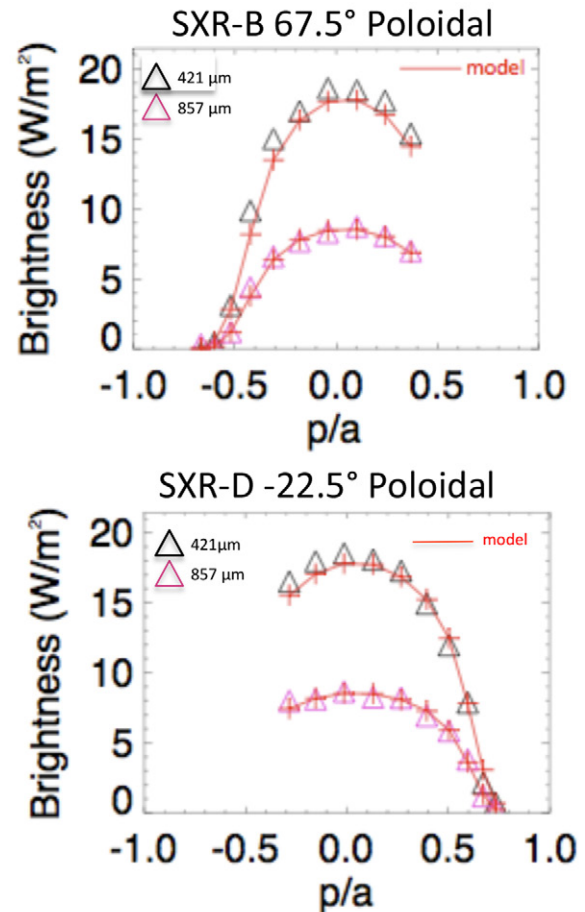

Figure 3. Measured (triangles) and modeled (plus signs) brightness through 421 μm (black) and 857 μm (purple) filters for two SXR detectors as a function of normalized impact parameter (proxy for radius). Model includes recombination radiation from intrinsic impurities previously described and Ar^{+18}. Similar level of agreement between model and data was found when including He^{+2} instead of Ar^{+18} in the model, and when only using impurity species measured by CHERS. Symbol size represents the uncertainty in the measured brightness.

in the model by adding an angular term of the same form. Previous measurements indicate a ring profile is a reasonable model because the impurity density profiles become hollow at the end of PPCD, the result of a temperature screening effect that expels impurities from the core [22]. Δn_C and Δn_{Al} are also input parameters with the ratios of the other impurity Δn's given by $\Delta n_O/\Delta n_C = 0.75$, $\Delta n_B/\Delta n_C = 0.3$, $\Delta n_N/\Delta n_c = 0.3$, and the Al states in ionization balance as before. The MCMC returns the distributions for the profile parameters. The most likely value for each parameter is found by taking the expectation value of the each distribution function.

For each set of profile parameters returned by the MCMC a profile is calculated for each included impurity species. Z_{eff} profiles are then calculated from those impurity profiles. This results in a distribution of Z_{eff} profiles. The peak of each distribution defines the most likely Z_{eff} and the width defines the uncertainty associated with Z_{eff} at each radial point.

A complete synthetic diagnostic for the CHERS system does not yet exist, therefore CHERS measurements were incorporated into the analysis through use of the prior distribution function.
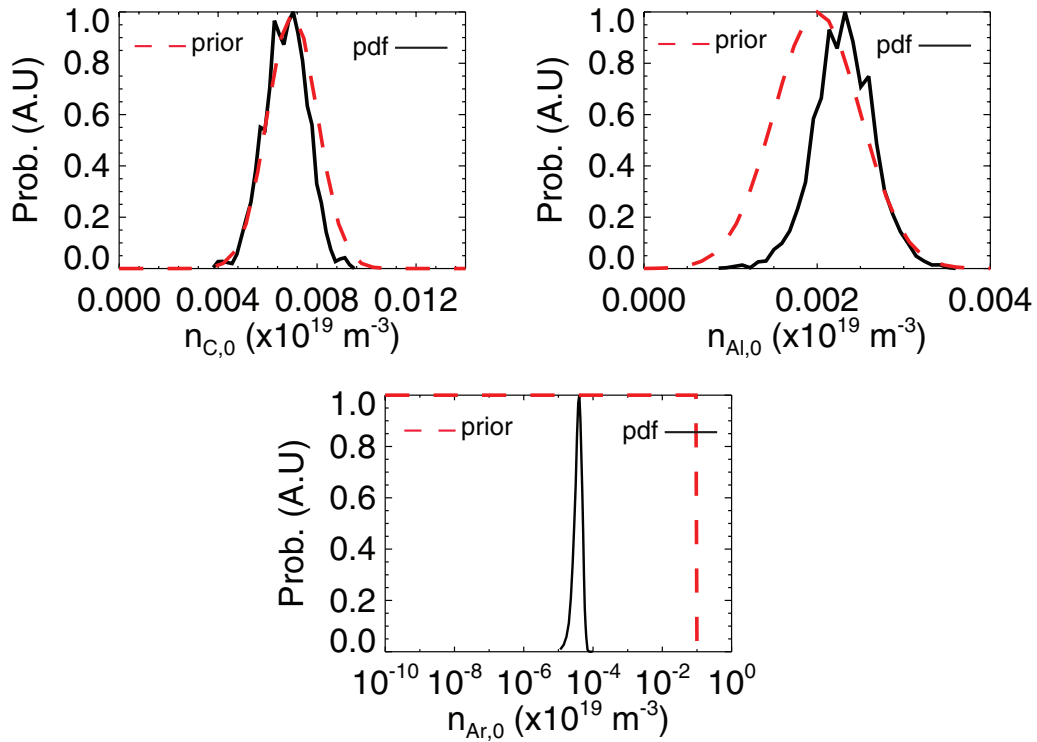
Figure 4. Posterior (solid black) and prior (dashed red) distributions for $n_{C,0}$, $n_{Al,0}$, and $n_{Ar,0}$. Note the logarithmic scale for the Ar distributions.
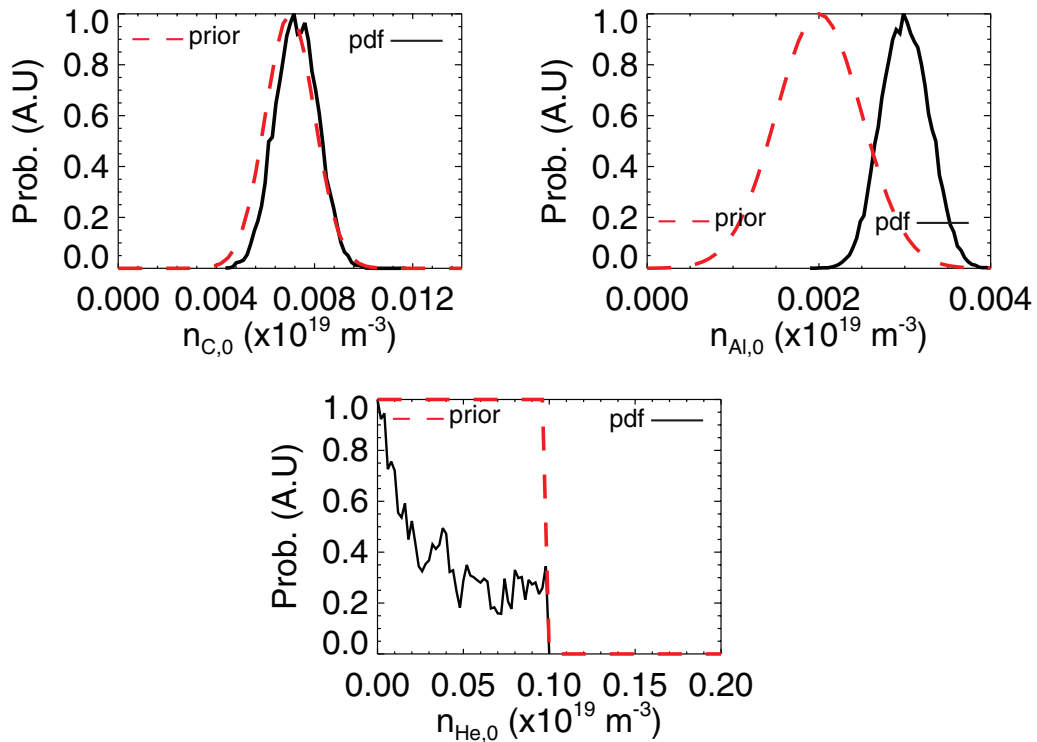
Figure 5. Posterior (solid black) and prior (dashed red) distributions for $n_{C,0}$, $n_{Al,0}$, and $n_{He,0}$.

Priors for the core and mid-radius density values were taken from CHERS measurements in similar discharges. The priors were Gaussians centered at the densities measured by CHERS, with widths of 15–25% of the maximum, slightly larger than the assumed uncertainty in the CHERS measurements, $\sim$10%. Uniform priors were assumed for the other four fit parameters.
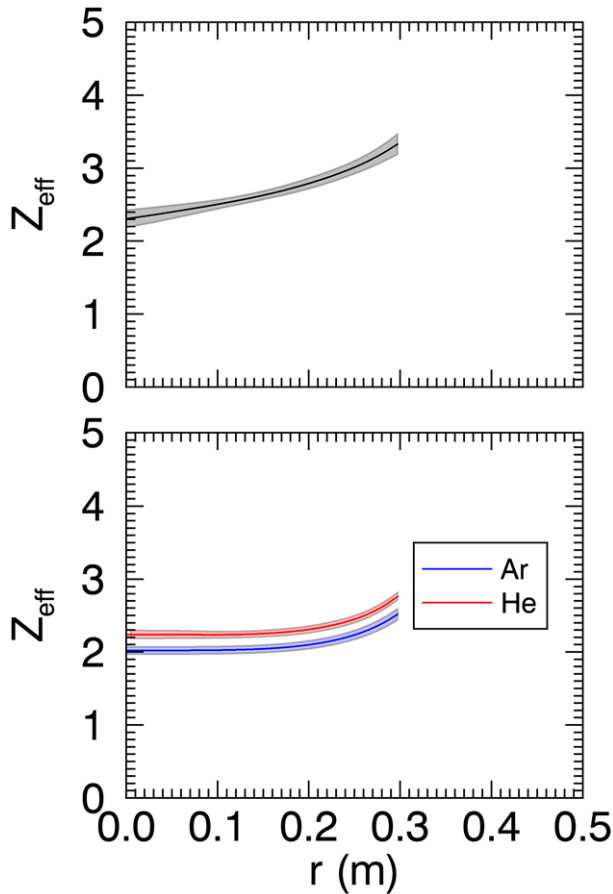
Figure 6. Z_{eff} profile determined by integration of SXR tomography and CHERS impurity measurements using only impurities measured by CHERS (top) and for two different test impurities and CHERS impurities (bottom) in modeling.

5. Application to 500 kA PPCD

The technique described above was applied to a set of high current ($I_p \sim 500$ kA) PPCD discharges with core line averaged $n_e \sim 0.75$–1.25×10^{19} m^{-3}. These discharges did not display significant 3D structures that are present in some MST plasmas. CHERS measurements in similar discharges provided a starting point for the impurity density profiles to begin the modeling. Two different unknown impurity parametric scans were undertaken, one with Ar^{+18} and one with He^{+2}, to make up any difference between the model and data not accounted for by the CHERS impurities. We do not expect Ar^{+18} to be present in unseeded discharges, however it serves as a proxy for other medium Z (>13) impurities, enabling us to test the relative sensitivity of the model to missing recombination emission. Due to the high Z of the species only a small amount is necessary to make a significant contribution to the modeled brightness, while leaving Z_{eff} relatively unchanged. A non-trivial amount of He is present in most MST discharges due to daily pulse discharge cleaning. However, the density of He, as well as its impact on the SXR signal, is unknown.

As illustrated in figure 3, the combination of bremsstrahlung and impurity recombination radiation produces very good agreement between the modeled (plus-signs) and measured brightness

(triangles). The slight under prediction of the thin filter data (black triangles) shown in figure 3 suggests extra, unaccounted for, emission in the low energy, <3 keV, region. This is most likely line radiation from medium Z impurities that is blocked by the thicker filters (purple triangles). However, the agreement between the thick filter model and data suggests that no additional density for the assumed impurities is needed to account for the thin filter disagreement. Thus, the value of Z_{eff} will not change when all sources of radiation are properly accounted for.

Figures 4 and 5 show posterior and prior distribution functions for core C^{+6}, Al^{+11}, Ar^{+18} and core C^{+6}, Al^{+11}, He^{+2} densities, respectively. Gaussian priors are used for both C^{+6} and Al^{+11} while uniform priors were used for Ar^{+18} and He^{+2}. Both parametric searches return C^{+6} and Al^{+11} densities that are consistent with the CHERS priors, though the Al^{+11} posterior distributions are much narrower than priors, indicating reduced uncertainty in the density. The estimated core Ar^{+18} density is consistent with levels possibly attributed to atmospheric contamination, shown in figure 4(c). This suggests that the SXR data reject the possibility of medium Z impurities other than Al being present in the plasma with sufficient density to contribute to Z_{eff} As illustrated in figure 5(c), the model predicts a non-zero core He^{+2} density. As previously stated, a non-negligible amount of He is expected in MST. The predicted density of He^{+2} is actually larger than the C^{+6} density, making it the dominate impurity in MST. However, due to the low Z of the species, this density of He does not significantly change Z_{eff} from a prediction with only impurities measured by CHERS. Additionally, all three cases, only CHERS impurities, CHERS plus Ar^{+18}, and CHERS plus He^{+2}, produce a very consistent value for Z_{eff}, approximately 2. Any additional impurities must be limited in density to explain the agreement between the SXR data and model with known impurities, thereby putting an upper bound on our determination of Z_{eff}.

As shown in figure 6, $Z_{eff} = 2.3 \pm 0.1$ in the core of these discharges, with a hollow radial profile peaking to $Z_{eff} = 3.3 \pm 0.2$ near mid-radius. The core value of Z_{eff} as determined from this method is in agreement with the estimate from CHERS only measurements in similar discharges [23]. As a result of using thick filters, 421 μm and 857 μm, the field of view of the SXR tomography system is limited to inside of $r \sim 0.3$ m. Thus, Z_{eff} cannot be determined outside of that radius from these data.

6. Conclusions and future work

This paper presents a method for determining Z_{eff} in MST from coupled SXR tomography and CHERS measurements using a Bayesian probability framework. Development of this method required modification of the existing SXR synthetic diagnostic to include additional sources of SXR emission, specifically impurity recombination radiation. The technique was applied to a set of high current, improved confinement discharges and shows core $Z_{eff} = 2.3 \pm 0.1$. This value is mutually consistent between both diagnostics, even when allowing for impurities not measured by CHERS, thus we have increased confidence that it is an accurate determination of Z_{eff} in a specific subset of MST discharges.

Future work will be devoted to incorporating additional diagnostics into the IDA framework. A synthetic diagnostic for CHERS is currently under development. This will provide a complete CHERS likelihood distribution function, which will refine the estimate for Z_{eff} in the IDA framework. Additional modifications to the SXR synthetic diagnostic are needed to account for high-energy line emission. This will enable the use of thinner filters which will expand the diagnostic field of view permitting characterization of the edge Z_{eff} and application of the diagnostic to standard MST discharges where the SXR emissivity is much lower.

Acknowledgments

References

[1] Anderson J.K. 2001 Measurement of the electrical resistivity profile in the Madison symmetric torus *PhD Thesis* University of Wisconsin-Madison

[2] Clayton D.J. 2010 Fast electron transport in improved confinement RFP plasmas *PhD Thesis* University of Wisconsin-Madison

[3] Clayton D.J., Almagri A.F., Burke D.R., Forest C.B., Goetz J.A., Kaufman M.C. and O'Connell R. 2010 An upgraded x-ray spectroscopy diagnostic on mst *Rev. Sci. Instrum.* **81** 10E308

[4] Fischer R., Wendland C., Dinklage A., Gori S., Dose V. and the W7-AS team 2002 Thomson scattering analysis with bayesian probability theory *Plasma Phys. Control. Fusion* **44** 1501–19

[5] Verdoolaege G., Fischer R. and Van Oost G. 2010 Potential of a bayesian integrated determination of the ion effective charge via bremmstrahlung and charge exchange spectroscopy in tokamak plasmas *IEEE Trans. Plasma Sci.* **38** 3168–96

[6] Rathgeber S.K. *et al* 2010 Estimation of profiles of the effective ion charge at asdex upgrade with integrated data analysis *Plasma Phys. Control. Fusion* **52** 095008

[7] van Milligen B.P., Estrada T., Ascasíbar E., Tafalla D., López-Bruna D., López A., Jiménez J.A., García-Cortés I., Dinklage A. and Fischer R. 2011 Integrated data analysis at TJ-II: the density profile *Rev. Sci. Instrum.* **82** 073503

[8] Dexter R.N., Kerst D.W., Lovell T.W., Prager S.C. and Sprott J.C. 1991 The madison symmetric torus *Fusion Technol.* **19** 131–9

[9] Sarff J.S., Hokin S., Ji H., Prager S.C. and Sovinec C.R. 1994 Fluctuation and transport reduction in a reversed filed pinch by inductive poloidal current drive *Phys. Rev. Lett.* **72** 3670–3

[10] Champan B.E. *et al* 2002 High confinement plasmas in the madison symmetric torus reversed-field pinch *Phys. Plasmas* **9** 2061

[11] McGarry M.B., Franz P., Den Hartog D.J. and Goetz J.A. 2010 A new double-foil soft x-ray array to measure T_e on the MST reversed field pinch *Rev. Sci. Instrum.* **81** 10E516

[12] Den Hartog D.J. *et al* 2006 Advances in neutral-beam-based diagnostics on the madison symmetric torus reversed-field pinch *Rev. Sci. Instrum.* **77** 10F122

[13] Gangadhara S., Craig D., Ennis D.A. and Den Hartog D.J. 2006 Modeling fast charge exchange recombiation spectroscopy measurements from the madison symmetric torus *Rev. Sci. Instrum.* **77** 10F109

[14] Craig D., Den Hartog D.J., Ennis D.A., Gangadhara S. and Holly D. 2007 High throughput spectrometer for fast localized doppler measurements *Rev. Sci. Instrum.* **78** 013103

[15] Kumar S.T.A., Den Hartog D.J., Champan B.E., O'Mullane M., Nornberg M., Craig D., Eilerman S., Fiksel G., Parke E. and Reusch J. 2012 High resolution charge-exchange spectroscopic measurements of aluminum impurity ions in a high temperature plasma *Plasma Phys. Control. Fusion* **54** 012002

[16] Sivia D.S. and Skilling J. 2006 *Data Analysis: a Bayesian Tutorial* 2nd edn (Oxford: Oxford University)

[17] Reusch L.M., Galante M.E., Franz P., Johnson J.R., McGarry M.B., Stephens H.D. and Den Hartog D.J. 2014 An integrated data analysis tool for improving measurements on the MST RFP *Rev. Sci. Instrum.* **85** 11D844

[18] Franz P., Marrelli L., Murari A., Spizzo G. and Martin P. 2001 Soft x ray tomographic imaging in the rfx reversed field pinch *Nucl. Fusion* **41** 695–709

[19] Von Goeler S., Stodiek W., Eubank H., Fishman H., Grebenshchikov S. and Hinnov E. 1975 Thermal x-ray spectra and impurities in the st tokamak *Nucl. Fusion* **15** 301–11

[20] Hutchinson I.H. 2002 *Principles of Plasma Diagnostics* (Cambridge: Cambridge University)

[21] Summers H.P. 2004 *The Atomic Data and Analysis Structure User Manual* version 2.6 www.adas.ac.uk

[22] Kumar S.T.A. *et al* 2012 Classical confinement and outward convection of impurity ions in the MST RFP *Phys. Plasmas* **19** 056121

[23] Barbui T., Carraro L., Den Hartog D.J., Kumar S.T.A. and Nornberg M. 2014 Impurity transport studies in the madison symmetric torus reversed-field pinch during standard and pulsed poloidal current drive regimes *Plasma Phys. Control. Fusion* **56** 075012